Magnon Crystallization in the Kagome Lattice Antiferromagnet

Jürgen Schnack,[1,*] Jörg Schulenburg,[2] Andreas Honecker,[3,†] and Johannes Richter[4,5,‡]
[1]Fakultät für Physik, Universität Bielefeld, Postfach 100131, D-33501 Bielefeld, Germany
[2]Universitätsrechenzentrum, Universität Magdeburg, D-39016 Magdeburg, Germany
[3]Laboratoire de Physique Théorique et Modélisation, CNRS UMR 8089, CY Cergy Paris Université, F-95302 Cergy-Pontoise Cedex, France
[4]Institut für Physik, Universität Magdeburg, P.O. Box 4120, D-39016 Magdeburg, Germany
[5]Max-Planck-Institut für Physik Komplexer Systeme, Nöthnitzer Straße 38, D-01187 Dresden, Germany

(Received 24 October 2019; accepted 10 August 2020; published 10 September 2020)

We present numerical evidence for the crystallization of magnons below the saturation field at nonzero temperatures for the highly frustrated spin-half kagome Heisenberg antiferromagnet. This phenomenon can be traced back to the existence of independent localized magnons or, equivalently, flatband multimagnon states. We present a loop-gas description of these localized magnons and a phase diagram of this transition, thus providing information for which magnetic fields and temperatures magnon crystallization can be observed experimentally. The emergence of a finite-temperature continuous transition to a magnon crystal is expected to be generic for spin models in dimension $D > 1$ where flatband multimagnon ground states break translational symmetry.

DOI: 10.1103/PhysRevLett.125.117207

Introduction.—Strongly correlated electronic spin systems may possess unusual and thus attractive properties such as magnetization curves characterized by sequences of magnetization plateaus with possible crystallization of magnons as reported for Cd-kapellasite recently [1]. This is of course a consequence of the intricate nature of their many-body eigenstates [2–5], which, however, for, e.g., Hubbard as well as Heisenberg models under special circumstances can express itself as destructive interference that "can lead to a disorder-free localization of particles" [6]. For translationally invariant systems this automatically yields flat bands in the single-particle energy spectrum, i.e., in one-magnon space in the case of spin Hamiltonians [7–14]. Today, flatband physics is investigated in several areas of physics, and many interesting phenomena that are related to flatbands have been found, see, e.g., Refs. [15–20]. Flatband systems can also be created using, e.g., cold atoms in optical lattices [21,22] or by employing photonic lattices [23–25].

Among the flatband systems, the highly frustrated quantum antiferromagnets (AFMs) play a particular role as possible solid-state realizations. There is a large variety of one-, two-, and three-dimensional lattices, where at high magnetic fields the lowest band of one-magnon excitations above the ferromagnetic vacuum is completely flat [26,27]. These flatband antiferromagnets exhibit several exotic features near saturation, such as a macroscopic magnetization jump at the saturation field [10], a magnetic-field driven spin-Peierls instability [28], a finite residual entropy at the saturation field [13,14,29], a very strong magnetocaloric effect [14,26,30], and an additional low-temperature maximum of the specific heat signaling the appearance of an additional low-energy scale [26].

The focus of the present Letter is on a prominent example of a flatband spin system, the spin-half kagome Heisenberg antiferromagnet (KHAF), that is a celebrated paradigm of highly frustrated quantum magnetism [2–5]. The corresponding Hamiltonian is given by

$$\underset{\sim}{H} = J \sum_{\{i<j\}} \underset{\sim}{\vec{s}_i} \cdot \underset{\sim}{\vec{s}_j} + g\mu_B B \sum_i \underset{\sim}{s_i^z}, \quad J > 0, \tag{1}$$

where the first term models the Heisenberg exchange between spins at nearest neighbor sites i and j and the second term provides the Zeeman splitting in an external magnetic field.

In addition to the widely debated character of the spin-liquid ground state (GS), the intriguing magnetization process of the KHAF has attracted much attention [1,10,13,14,26,28,29,31–40]. The magnetization exhibits plateaus at certain fractions of the saturation magnetization, namely at $\mathcal{M}/\mathcal{M}_{\mathrm{sat}} = 3/9 = 1/3, 5/9, 7/9$ and likely also at $\mathcal{M}/\mathcal{M}_{\mathrm{sat}} = 1/9$ [34,35]. In contrast to the semiclassical $\mathcal{M}/\mathcal{M}_{\mathrm{sat}} = 1/3$ plateau in the triangular-lattice Heisenberg antiferromagnet, see, e.g., Refs. [41–43], the kagome plateau states are quantum valence-bond states [13,14,28,33–35]. Moreover, around the $\mathcal{M}/\mathcal{M}_{\mathrm{sat}} = 7/9$–plateau the flat lowest one-magnon band [10] dominates the low-temperature physics and leads to the exotic properties mentioned above. Interestingly, the $\mathcal{M}/\mathcal{M}_{\mathrm{sat}} = 7/9$ plateau state just below the jump to saturation is a magnon crystal that is the magnetic counterpart of the Wigner crystal of interacting

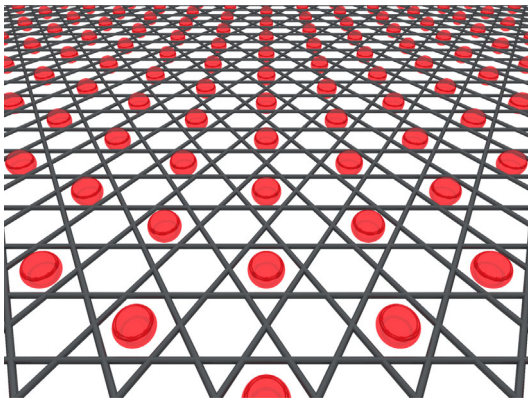

FIG. 1. Sketch of the crystal of localized magnons (of minimal size) on the kagome lattice antiferromagnet. These localized magnons (red discs) are superpositions of spin flips of spins residing at the vertices of the confining basic hexagons of the kagome lattice.

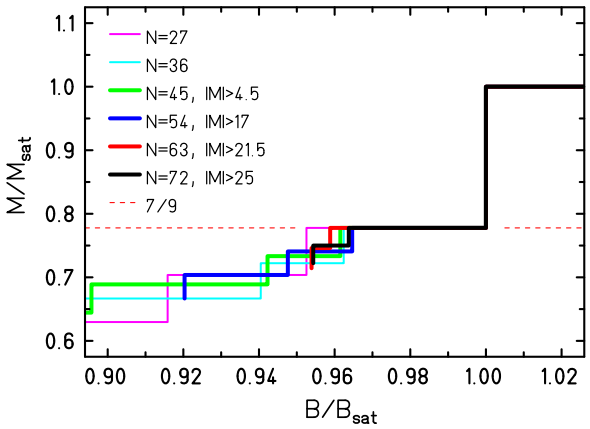

FIG. 2. Magnetization $\mathcal{M}/\mathcal{M}_{\mathrm{sat}}$: Region of the $7/9$ plateau for various finite-size realizations of the KHAF.

electrons in two dimensions. Since the magnon crystal spontaneously breaks translational symmetry, a finite-temperature phase transition is possible. The challenge is to find appropriate theoretical tools to describe such a transition for the quantum many-body system at hand.

Remarkably, the very existence of a flat band allows a semirigorous analysis of the low-temperature physics, e.g., for most of the one-dimensional flatband quantum spin systems including the sawtooth chain [14,29,30] and also for a few two-dimensional systems, such as the frustrated bilayer [6,44,45], as well as the Tasaki lattice [46]. Such a semi-rigorous analysis builds on the existence of compact localized many-magnon states, which form either a massively degenerate GS manifold at the saturation field B_{sat} or a huge set of low-lying excitations for $B \lesssim B_{\mathrm{sat}}$ and $B \gtrsim B_{\mathrm{sat}}$. For the KHAF, the compact localized many-magnon states live on nontouching hexagons [10], which can be mapped to hard hexagons on a triangular lattice [13,14,26,29]. This situation is depicted in Fig. 1.

On the experimental side the growing number of kagome compounds is promising with respect to possible solid-state realizations of the kagome flatband physics [47–55]. Very recently the magnetization process in high field was reported for Cd-kapellasite [1]. The authors interpret the observed plateau states "as crystallizations of emergent magnons localized on the hexagon of the kagome lattice." We will address the relation to our investigations in the discussion below.

Reliable predictions of the field-temperature regions where the magnon-crystal phase exists are useful to stimulate specific experiments. However, the semi-rigorous analysis of the flatband properties of the KHAF based on compact localized many-magnon states, i.e., the hard-hexagon approximation (HHA) is limited because of the existence of a macroscopic number of additional *non-compact* localized many-magnon states [27]. A complete description can be given in terms of a loop gas (LG) that we elaborate in the Supplemental Material [56]. Moreover, at nonzero temperature also nonlocalized eigenstates influence the thermodynamics of the KHAF.

Numerical method.—To investigate the KHAF near the saturation field we present large-scale exact-diagonalization (ED) studies using the finite-temperature Lanczos (FTL) method for finite lattices of $N = 27, \ldots, 72$ sites, where we have selected only lattices exhibiting the magnon-crystal plateau at $\mathcal{M}/\mathcal{M}_{\mathrm{sat}} = 7/9$, which excludes $N = 42$ discussed in Ref. [37]. FTL is an unbiased numerical approach by which thermodynamic quantities are very accurately approximated by means of trace estimators [57–62]. Moreover, the consideration of six different lattices up to $N = 72$ allows us to estimate finite-size effects. For used lattices and technical details see Ref. [56]. The kagome lattices of N sites correspond to triangular lattices of $N_{\mathrm{trian}} = N/3$ sites. On symmetry grounds, triangular lattices of $N_{\mathrm{trian}} = 9$, 12, 21, i.e., $N = 27$, 36, 63 sites seem to be most appropriate for our investigation [56,63].

Results.—The magnetization curve around the $7/9$ plateau and the jump to saturation are shown in Fig. 2. The size independence of the height of the jump is obvious. The width of the plateau, i.e., the field region where the magnon-crystal phase can exist, is about 4% of the saturation field and its finite-size dependence is weak, cf. Ref. [35]. The finite-temperature transition to the magnon-crystal phase can be driven either by temperature when fixing B in the plateau region or by the magnetic field when fixing T below the critical temperature T_c. $C(B, T)$ is an appropriate quantity to detect the transition. For finite lattices the specific heat will not exhibit a true singularity, rather we may expect a well-pronounced peak in C that indicates the critical point. Furthermore, the peak has to become sharper with increasing N.

First, we study the temperature profile $C(T)$ for a magnetic field slightly below saturation, $B = 0.99B_{\mathrm{sat}}$ (see Fig. 3). While the influence of N on the peak position

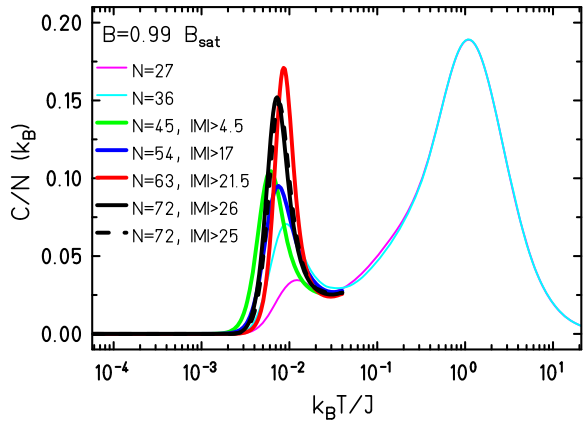

FIG. 3. Specific heat for $B = 0.99B_{\mathrm{sat}}$ for various finite-size realizations of the KHAF. For $N = 45, 54, 63, 72$, where too large Hilbert subspaces had to be neglected, only the low-temperature part of the specific heat is displayed; it is virtually exact for all system sizes.

T_{max} is rather weak, the increase of the height C_{max} with growing N is significant and the peaks are sharpest for $N = 63$ and $N = 72$.

Figure 4 presents a closer look at the results of Fig. 3 in terms of some characteristic quantities where we include the HHA [13,14] and the LG description [56] for comparison. In panel (a) we first present a comparison of the total ground-state entropy per site. Since hard hexagons are a subset of the loop configurations that in turn are a subset of the KHA ground states, the values of S increase correspondingly for a fixed N. For the HHA, the result for the thermodynamic limit is known [13,14,64] and shown by the horizontal blue line. We note that the result

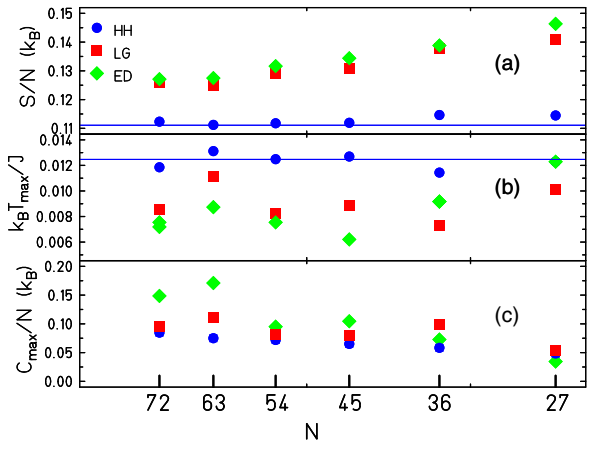

FIG. 4. System-size dependence of several characteristic quantities at $B = 0.99B_{\mathrm{sat}}$ for HH approximation, LG, and ED: (a) entropy per site S/N associated to the total ground-state degeneracy, (b) position of the maximum of the specific heat T_{max}, and (c) value of the maximum of the specific heat per site C_{max}/N. The horizontal blue lines in panels (a) and (b) show the known thermodynamic limit for hard hexagons [13,14,64,65].

for $N = 63$ within the HHA is very close to this $N = \infty$ limit. Since the finite-size effects of the LG and the KHA are very similar to that of the HHA, we assume that also for these models a system size of $N \geq 63$ is at least necessary to arrive at trustworthy results. It is thus a major achievement that by means of FTL such sizes are accessible.

We observe furthermore that nested loop configurations do indeed give rise to another macroscopic contribution to the ground states [27], and while this is approaching the ED result for the KHA, there is yet another contribution to the ground-state manifold that does not come from localized magnons and thus cannot be captured by the LG either.

Figure 4(b) displays the size dependence of the position of the maximum T_{max} of the specific heat in all three approximations. The thermodynamic limit of the HHA is again known [13,14,65] and again shown by the horizontal blue line. The positions for $N \gtrsim 45$ scatter around this value, and since the finite-size effects of all three approaches are again similar, we assume the same to be true for the LG and the KHA. Thus, we conclude that the critical temperature is lowered by the higher ground-state degeneracy of the LG and the KHA by up to 50% as compared to the HHA even for a field as close to the saturation field as $B = 0.99B_{\mathrm{sat}}$.

Finally, Fig. 4(c) shows the size dependence of C_{max}/N. The range of accessible system sizes and lattice geometries is too small to reliably extract critical exponents, but one does observe a trend of C_{max}/N to grow with increasing system size N. To be more precise, the transition is expected to belong to the universality class of the classical two-dimensional three-state Potts model [13,14] for all three cases. Thus, the asymptotic behavior of C_{max}/N for large N should be given by $C_{\mathrm{max}}/N \propto N^{(\alpha/2\nu)}$ [66] with critical indices $\alpha = 1/3$ and $\nu = 5/6$ [67,68].

Next, we consider the field dependence of the specific heat for a representative low temperature $T/J = 0.01$, see Fig. 5, where we present data for $N = 63$ (solid curves). For the HHA, we include the result for the thermodynamic limit $N = \infty$ [13,14,65] (dashed curve). We note that both the HHA and the LG scale with $(B - B_{\mathrm{sat}})/T$ [13,14,26]. There are two peaks left and right of the minimum in $C(B)$ at $B = B_{\mathrm{sat}}$ which are related to the ground states of Fig. 4(a). The curves for $N = 63$ and ∞ of the HHA for the peak at $B > B_{\mathrm{sat}}$ are indistinguishable, showing that this is not a phase transition. The peaks of the LG and ED for $B > B_{\mathrm{sat}}$ are at almost the same position but higher than for the HHA, and they do not signal a phase transition either. Remarkably, the LG is very close to the ED result for $B > B_{\mathrm{sat}}$, a fact that can be attributed to the LG reproducing the exact ground-state degeneracy of the highest sectors of total magnetic quantum number for the KHAF, see also Ref. [56].

Turning to the region $B < B_{\mathrm{sat}}$ of Fig. 5, here the HHA is known to exhibit a phase transition [13,14,65] whose location is given by the divergence of the $N = \infty$ curve

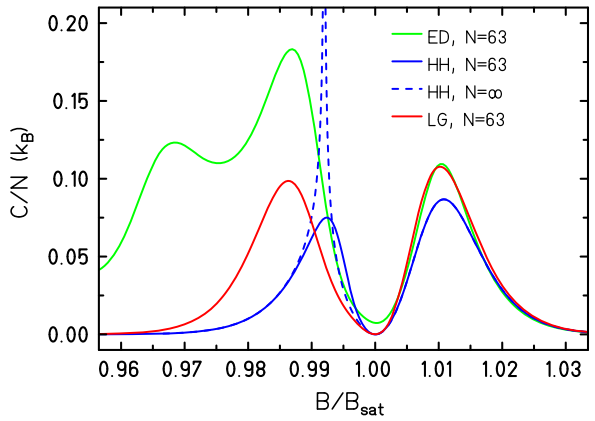

FIG. 5. Specific heat vs B at $T/J = 0.01$ for the KHAF, HH approximation, and LG with $N = 63$ (solid curves) and the thermodynamic limit of hard hexagons [13,14,65] (dashed curve).

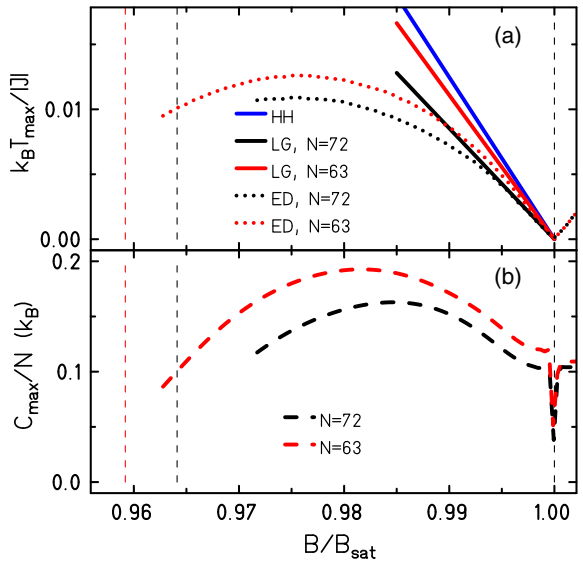

FIG. 6. Phase diagram: (a) Position $T_{\max}$ and (b) height $C_{\max}$ of the low-T maximum (cf. Fig. 3) in dependence on B for $N = 63$ and $N = 72$ for fields where the maximum can be unambiguously detected. The vertical dashed lines mark the respective edges of the magnetization plateau.

(dashed). The peaks in the ED and LG curves just below $0.99B_{\text{sat}}$ should correspond to the same crystallization transition, they are just rounded off by the finite size and pushed to lower B compared to the HHA by the larger number of states involved. In this region, the ED peak is higher than that of the LG. This difference is not only due to the KHAF having ground states that have no LG description [56], but also due to low-lying excitations. The latter give rise to a second peak at $0.97B_{\text{sat}}$ that is present only in the ED data.

To derive a tentative phase diagram, we show in Fig. 6(a) the position $T_{\max}$ of the low-T peak of $C(T)$ vs B for $N = 63$ and $N = 72$. We also show the HHA result $T_c = 0.928(1 - B/B_{\text{sat}})$ for $N = \infty$ [13,14] and the LG curves for $N = 63$ and 72 (straight lines). The LG curves are very close to tangential to the corresponding ED results just below the saturation field, while the HHA yields a higher transition temperature, as already noticed in the context of Fig. 4(b). As B decreases, the ED curves bend down, and when approaching the lower end point B_{end} of the plateau (depicted by the vertical lines in Fig. 6) $T_{\max}$ decreases and we may expect that it vanishes near B_{end}, where the magnon-crystal ground state disappears. For finite systems, as approaching B_{end} the relevant peak in $C(T)$ merges with low-T finite-size peaks appearing just below B_{end}, this way masking the true behavior expected for $N \to \infty$.

We mention that the general shape of the transition curve in Fig. 6(a) resembles the phase diagram of the magnon crystallization of the fully frustrated bilayer AFM [6,44,45]. Therefore, we may argue that the shape of this curve is generic for two-dimensional spin models possessing flatband multimagnon ground states.

The height of the maximum $C_{\max}$ of $C(T)$ (supposed to become a power-law singularity for $N \to \infty$) is shown in Fig. 6(b) vs B for $N = 63$ and $N = 72$. The shape of these curves is domelike with a maximum near the midpoint of the plateau. The unusual behavior at $B = B_{\text{sat}}$ is discussed in Ref. [26].

Discussion.—Our FTL data confirm the very existence of a low-temperature magnon-crystal phase just below the saturation field as conjectured by the HHA [13,14]. However, the $B - T$ region where this phase exists is not properly described by the HHA. Instead we elaborated a LG description that complements our FTL investigations. It is very accurate for $B > B_{\text{sat}}$ and still yields a good description just below B_{sat}. Our investigations therefore provide guidance in which range of field and temperature a magnon-crystal phase is to be expected.

Coming back to the "magnon crystallization" reported in the experimental paper [1]: Here the authors interpret the observed plateau states as crystallizations of emergent magnons localized on the hexagon of the kagome lattice. This concept coincides with the present study for the 7/9 plateau, but may differ for plateaus at smaller magnetization, e.g., at 1/3 and 5/9. Although these lower plateaus can be understood as magnon crystals formed at $T = 0$, it still has to be investigated whether the physical behavior for $T > 0$ differs from the scenario discussed in this Letter, since the huge set of flatband multimagnon states determining the low-T thermodynamics near B_{sat} is missing for these plateaus.

As already discussed by the authors of Ref. [1] a real compound always differs from the idealized theoretical case, for instance, due to long-range dipolar or Dzyaloshinskii-Moriya interactions. In the case of Cd-kapellasite these seem to stabilize a phase at 10/12 of the saturation magnetization. However, the structure of this phase appears to be rather similar to that at 7/9, it therefore served as a strong motivation to investigate the possibility

of a magnon crystallization phase transition on very general grounds (and with an idealized Hamiltonian). The effect of certain anisotropic Hamiltonians on magnon crystal phases confined to kagome stripes is extensively discussed in, e.g., Ref. [40].

This work was supported by the Deutsche Forschungsgemeinschaft (DFG SCHN 615/23-1). Computing time at the Leibniz Center in Garching is gratefully acknowledged. The authors are indebted to O. Derzhko, J. Strečka, and M. E. Zhitomirsky for valuable discussions.

*jschnack@uni-bielefeld.de
†andreas.honecker@cyu.fr
‡Johannes.Richter@physik.uni-magdeburg.de

[1] R. Okuma, D. Nakamura, T. Okubo, A. Miyake, A. Matsuo, K. Kindo, M. Tokunaga, N. Kawashima, S. Takeyama, and Z. Hiroi, A series of magnon crystals appearing under ultrahigh magnetic fields in a kagomé antiferromagnet, Nat. Commun. **10**, 1229 (2019).
[2] L. Balents, Spin liquids in frustrated magnets, Nature (London) **464**, 199 (2010).
[3] O. A. Starykh, Unusual ordered phases of highly frustrated magnets: A review, Rep. Prog. Phys. **78**, 052502 (2015).
[4] P. Mendels and F. Bert, Quantum kagome frustrated antiferromagnets: One route to quantum spin liquids, C.R. Phys. **17**, 455 (2016).
[5] L. Savary and L. Balents, Quantum spin liquids, Rep. Prog. Phys. **80**, 016502 (2017).
[6] J. Richter, O. Krupnitska, V. Baliha, T. Krokhmalskii, and O. Derzhko, Thermodynamic properties of $Ba_2CoSi_2O_6Cl_2$ in a strong magnetic field: Realization of flat-band physics in a highly frustrated quantum magnet, Phys. Rev. B **97**, 024405 (2018).
[7] A. Mielke, Ferromagnetic ground states for the Hubbard model on line graphs, J. Phys. A **24**, L73 (1991).
[8] H. Tasaki, Ferromagnetism in the Hubbard Models with Degenerate Single-Electron Ground States, Phys. Rev. Lett. **69**, 1608 (1992).
[9] J. Schnack, H.-J. Schmidt, J. Richter, and J. Schulenburg, Independent magnon states on magnetic polytopes, Eur. Phys. J. B **24**, 475 (2001).
[10] J. Schulenburg, A. Honecker, J. Schnack, J. Richter, and H.-J. Schmidt, Macroscopic Magnetization Jumps due to Independent Magnons in Frustrated Quantum Spin Lattices, Phys. Rev. Lett. **88**, 167207 (2002).
[11] S. A. Blundell and M. D. Núñez-Regueiro, Quantum topological excitations: From the sawtooth lattice to the Heisenberg chain, Eur. Phys. J. B **31**, 453 (2003).
[12] J. Richter, J. Schulenburg, A. Honecker, J. Schnack, and H.-J. Schmidt, Exact eigenstates and macroscopic magnetization jumps in strongly frustrated spin lattices, J. Phys. Condens. Matter **16**, S779 (2004).
[13] M. E. Zhitomirsky and H. Tsunetsugu, Exact low-temperature behavior of a kagomé antiferromagnet at high fields, Phys. Rev. B **70**, 100403(R) (2004).
[14] M. E. Zhitomirsky and H. Tsunetsugu, High field properties of geometrically frustrated magnets, Prog. Theor. Phys. Suppl. **160**, 361 (2005).
[15] S. D. Huber and E. Altman, Bose condensation in flat bands, Phys. Rev. B **82**, 184502 (2010).
[16] S. A. Parameswaran, R. Roy, and S. L. Sondhi, Fractional quantum Hall physics in topological flat bands, C.R. Phys. **14**, 816 (2013).
[17] E. J. Bergholtz and Z. Liu, Toplogical flat band models and fractional Chern insulators, Int. J. Mod. Phys. B **27**, 1330017 (2013).
[18] D. Leykam, S. Flach, O. Bahat-Treidel, and A. S. Desyatnikov, Flat band states: Disorder and nonlinearity, Phys. Rev. B **88**, 224203 (2013).
[19] O. Derzhko, J. Richter, and M. Maksymenko, Strongly correlated flat-band systems: The route from Heisenberg spins to Hubbard electrons, Int. J. Mod. Phys. B **29**, 1530007 (2015).
[20] D. Leykam, A. Andreanov, and S. Flach, Artificial flat band systems: from lattice models to experiments, Adv. Phys. X **3**, 1473052 (2018).
[21] G.-B. Jo, J. Guzman, C. K. Thomas, P. Hosur, A. Vishwanath, and D. M. Stamper-Kurn, Ultracold Atoms in a Tunable Optical Kagome Lattice, Phys. Rev. Lett. **108**, 045305 (2012).
[22] J. Struck, C. Ölschläger, M. Weinberg, P. Hauke, J. Simonet, A. Eckardt, M. Lewenstein, K. Sengstock, and P. Windpassinger, Tunable Gauge Potential for Neutral and Spinless Particles in Driven Optical Lattices, Phys. Rev. Lett. **108**, 225304 (2012).
[23] R. A. Vicencio, C. Cantillano, L. Morales-Inostroza, B. Real, C. Mejía-Cortés, S. Weimann, A. Szameit, and M. I. Molina, Observation of Localized States in Lieb Photonic Lattices, Phys. Rev. Lett. **114**, 245503 (2015).
[24] S. Mukherjee, A. Spracklen, D. Choudhury, N. Goldman, P. Öhberg, E. Andersson, and R. R. Thomson, Observation of a Localized Flat-Band State in a Photonic Lieb Lattice, Phys. Rev. Lett. **114**, 245504 (2015).
[25] F. Baboux, L. Ge, T. Jacqmin, M. Biondi, E. Galopin, A. Lemaître, L. Le Gratiet, I. Sagnes, S. Schmidt, H. E. Türeci, A. Amo, and J. Bloch, Bosonic Condensation and Disorder-Induced Localization in a Flat Band, Phys. Rev. Lett. **116**, 066402 (2016).
[26] O. Derzhko and J. Richter, Universal low-temperature behavior of frustrated quantum antiferromagnets in the vicinity of the saturation field, Eur. Phys. J. B **52**, 23 (2006).
[27] O. Derzhko, J. Richter, A. Honecker, and H.-J. Schmidt, Universal properties of highly frustrated quantum magnets in strong magnetic fields, Low Temp. Phys. **33**, 745 (2007).
[28] J. Richter, O. Derzhko, and J. Schulenburg, Magnetic-Field Induced Spin-Peierls Instability in Strongly Frustrated Quantum Spin Lattices, Phys. Rev. Lett. **93**, 107206 (2004).
[29] O. Derzhko and J. Richter, Finite low-temperature entropy of some strongly frustrated quantum spin lattices in the vicinity of the saturation field, Phys. Rev. B **70**, 104415 (2004).
[30] M. E. Zhitomirsky and A. Honecker, Magnetocaloric effect in one-dimensional antiferromagnets, J. Stat. Mech. (2004) P07012.
[31] K. Hida, Magnetization process of the $S = 1$ and $1/2$ uniform and distorted Kagomé Heisenberg antiferromagnets, J. Phys. Soc. Jpn. **70**, 3673 (2001).

[32] A. Honecker, J. Schulenburg, and J. Richter, Magnetization plateaus in frustrated antiferromagnetic quantum spin models, J. Phys. Condens. Matter **16**, S749 (2004).

[33] D. C. Cabra, M. D. Grynberg, P. C. W. Holdsworth, A. Honecker, P. Pujol, J. Richter, D. Schmalfuß, and J. Schulenburg, Quantum kagomé antiferromagnet in a magnetic field: Low-lying nonmagnetic excitations versus valence-bond crystal order, Phys. Rev. B **71**, 144420 (2005).

[34] S. Nishimoto, N. Shibata, and C. Hotta, Controlling frustrated liquids and solids with an applied field in a kagome Heisenberg antiferromagnet, Nat. Commun. **4**, 2287 (2013).

[35] S. Capponi, O. Derzhko, A. Honecker, A. M. Läuchli, and J. Richter, Numerical study of magnetization plateaus in the spin-$\frac{1}{2}$ kagome Heisenberg antiferromagnet, Phys. Rev. B **88**, 144416 (2013).

[36] H. Nakano and T. Sakai, Numerical-diagonalization study of magnetization process of frustrated spin-1/2 Heisenberg antiferromagnets in two dimensions:—Triangular- and kagome-lattice antiferromagnets—, J. Phys. Soc. Jpn. **87**, 063706 (2018).

[37] J. Schnack, J. Schulenburg, and J. Richter, Magnetism of the $N = 42$ kagome lattice antiferromagnet, Phys. Rev. B **98**, 094423 (2018).

[38] X. Chen, S.-J. Ran, T. Liu, C. Peng, Y.-Z. Huang, and G. Su, Thermodynamics of spin-1/2 Kagomé Heisenberg antiferromagnet: Algebraic paramagnetic liquid and finite-temperature phase diagram, Sci. Bull. **63**, 1545 (2018).

[39] K. Morita, T. Sugimoto, S. Sota, and T. Tohyama, Magnetization plateaus in the spin-$\frac{1}{2}$ antiferromagnetic Heisenberg model on a kagome-strip chain, Phys. Rev. B **97**, 014412 (2018).

[40] S. Acevedo, C. A. Lamas, M. Arlego, and P. Pujol, Magnon crystals and magnetic phases in a kagome-stripe antiferromagnet, Phys. Rev. B **100**, 195145 (2019).

[41] A. V. Chubukov and D. I. Golosov, Quantum theory of an antiferromagnet on a triangular lattice in a magnetic field, J. Phys. Condens. Matter **3**, 69 (1991).

[42] A. Honecker, A comparative study of the magnetization process of two-dimensional antiferromagnets, J. Phys. Condens. Matter **11**, 4697 (1999).

[43] D. J. J. Farnell, R. Zinke, J. Schulenburg, and J. Richter, High-order coupled cluster method study of frustrated and unfrustrated quantum magnets in external magnetic fields, J. Phys. Condens. Matter **21**, 406002 (2009).

[44] F. Alet, K. Damle, and S. Pujari, Sign-Problem-Free Monte Carlo Simulation of Certain Frustrated Quantum Magnets, Phys. Rev. Lett. **117**, 197203 (2016).

[45] O. Derzhko, T. Krokhmalskii, and J. Richter, Emergent Ising degrees of freedom in frustrated two-leg ladder and bilayer $s = \frac{1}{2}$ Heisenberg antiferromagnets, Phys. Rev. B **82**, 214412 (2010).

[46] M. Maksymenko, A. Honecker, R. Moessner, J. Richter, and O. Derzhko, Flat-Band Ferromagnetism as a Pauli-Correlated Percolation Problem, Phys. Rev. Lett. **109**, 096404 (2012).

[47] J. L. Atwood, Kagomé lattice–A molecular toolkit for magnetism, Nat. Mater. **1**, 91 (2002).

[48] P. Mendels, F. Bert, M. A. de Vries, A. Olariu, A. Harrison, F. Duc, J. C. Trombe, J. S. Lord, A. Amato, and C. Baines, Quantum Magnetism in the Paratacamite Family: Towards an Ideal Kagomé Lattice, Phys. Rev. Lett. **98**, 077204 (2007).

[49] F. Bert, S. Nakamae, F. Ladieu, D. L'Hôte, P. Bonville, F. Duc, J.-C. Trombe, and P. Mendels, Low temperature magnetization of the $S = \frac{1}{2}$ kagome antiferromagnet $ZnCu_3(OH)_6Cl_2$, Phys. Rev. B **76**, 132411 (2007).

[50] Y. Okamoto, M. Tokunaga, H. Yoshida, A. Matsuo, K. Kindo, and Z. Hiroi, Magnetization plateaus of the spin-$\frac{1}{2}$ kagome antiferromagnets volborthite and vesignieite, Phys. Rev. B **83**, 180407(R) (2011).

[51] T.-H. Han, J. S. Helton, S. Chu, D. G. Nocera, J. A. Rodriguez-Rivera, C. Broholm, and Y. S. Lee, Fractionalized excitations in the spin-liquid state of a kagome-lattice antiferromagnet, Nature (London) **492**, 406 (2012).

[52] K. Katayama, N. Kurita, and H. Tanaka, Quantum phase transition between disordered and ordered states in the spin-$\frac{1}{2}$ kagome lattice antiferromagnet $(Rb_{1-x}Cs_x)_2Cu_3SnF_{12}$, Phys. Rev. B **91**, 214429 (2015).

[53] H. Ishikawa, M. Yoshida, K. Nawa, M. Jeong, S. Krämer, M. Horvatić, C. Berthier, M. Takigawa, M. Akaki, A. Miyake, M. Tokunaga, K. Kindo, J. Yamaura, Y. Okamoto, and Z. Hiroi, One-Third Magnetization Plateau with a Preceding Novel Phase in Volborthite, Phys. Rev. Lett. **114**, 227202 (2015).

[54] M. R. Norman, Colloquium: Herbertsmithite and the search for the quantum spin liquid, Rev. Mod. Phys. **88**, 041002 (2016).

[55] M. Yoshida, K. Nawa, H. Ishikawa, M. Takigawa, M. Jeong, S. Krämer, M. Horvatić, C. Berthier, K. Matsui, T. Goto, S. Kimura, T. Sasaki, J. Yamaura, H. Yoshida, Y. Okamoto, and Z. Hiroi, Spin dynamics in the high-field phases of volborthite, Phys. Rev. B **96**, 180413(R) (2017).

[56] See Supplemental Material at http://link.aps.org/supplemental/10.1103/PhysRevLett.125.117207 for structures of investigated lattices, in-depth evaluations of the loop-gas model, tables of degeneracies, and additional figures comparing the specific heat for various lattice sizes.

[57] J. Jaklič and P. Prelovšek, Lanczos method for the calculation of finite-temperature quantities in correlated systems, Phys. Rev. B **49**, 5065(R) (1994).

[58] J. Schnack and O. Wendland, Properties of highly frustrated magnetic molecules studied by the finite-temperature Lanczos method, Eur. Phys. J. B **78**, 535 (2010).

[59] O. Hanebaum and J. Schnack, Advanced finite-temperature Lanczos method for anisotropic spin systems, Eur. Phys. J. B **87**, 194 (2014).

[60] B. Schmidt and P. Thalmeier, Frustrated two dimensional quantum magnets, Phys. Rep. **703**, 1 (2017).

[61] P. Prelovšek, The finite temperature Lanczos method and its applications, in *The Physics of Correlated Insulators, Metals, and Superconductors*, edited by E. Pavarini, E. Koch, R. Scalettar, and R. Martin (2017), http://hdl.handle.net/2128/15283.

[62] J. Schnack, J. Richter, and R. Steinigeweg, Accuracy of the finite-temperature Lanczos method compared to simple typicality-based estimates, Phys. Rev. Research **2**, 013186 (2020).

[63] B. Bernu, C. Lhuillier, and L. Pierre, Signature of Néel Order in Exact Spectra of Quantum Antiferromagnets on Finite Lattices, Phys. Rev. Lett. **69**, 2590 (1992).
[64] R. J. Baxter and S. K. Tsang, Entropy of hard hexagons, J. Phys. A **13**, 1023 (1980).
[65] R. J. Baxter, Hard hexagons: Exact solution, J. Phys. A **13**, L61 (1980).
[66] J.-K. Kim and D. P. Landau, Corrections to finite-size-scaling in two dimensional Potts models, Physica (Amsterdam) **250A**, 362 (1998).
[67] F. Y. Wu, The Potts model, Rev. Mod. Phys. **54**, 235 (1982).
[68] T. Nagai, Y. Okamoto, and W. Janke, Crossover scaling in the two-dimensional three-state Potts model, Condens. Matter Phys. **16**, 23605 (2013).